NASA TECHNICAL NOTE

NASA TN D-3544

c. 1

LOAN COPY: RETU
AFWL (WLIL-
KIRTLAND AFB, N

TECH LIBRARY KAFB, NM
0130279

NASA TN D-3544

STATIC STABILITY CHARACTERISTICS OF CONE AND HALF-CONE–PYRAMID CONFIGURATIONS AT MACH 6.83

by Peter T. Bernot and Bruce C. Jordan

Langley Research Center
Langley Station, Hampton, Va.

RECEIVED
6 SEP 1966
Technical Library
Air Force Weapons
Laboratory

NATIONAL AERONAUTICS AND SPACE ADMINISTRATION • WASHINGTON, D. C. • AUGUST 1966

TECH LIBRARY KAFB, NM
0130279

NASA TN D-3544

STATIC STABILITY CHARACTERISTICS OF CONE AND HALF-CONE—PYRAMID CONFIGURATIONS AT MACH 6.83

By Peter T. Bernot and Bruce C. Jordan

Langley Research Center
Langley Station, Hampton, Va.

NATIONAL AERONAUTICS AND SPACE ADMINISTRATION

For sale by the Clearinghouse for Federal Scientific and Technical Information
Springfield, Virginia 22151 – Price $2.00

STATIC STABILITY CHARACTERISTICS OF CONE AND HALF-CONE—PYRAMID CONFIGURATIONS AT MACH 6.83

By Peter T. Bernot and Bruce C. Jordan
Langley Research Center

SUMMARY

The longitudinal and lateral stability characteristics of a 5° semivertex angle cone and a D-body consisting of a half-cone of 5° semivertex angle with a rectangular pyramid were determined at a Mach number of 6.83 and a Reynolds number of 1.45×10^6. These bodies were also tested in conjunction with a delta wing swept back 83.3°. The D-body configurations were tested in the flat-bottom and flat-top orientations. Effects of Reynolds number variation on the cone model were also investigated.

For the 5° cone model, predictions of Newtonian theory plus skin-friction estimates were in good agreement with the experimental values of the maximum lift-drag ratio $(L/D)_{max}$ obtained at Reynolds numbers from 0.76×10^6 to 3.00×10^6. Very good agreement between measured values of minimum drag coefficient and predictions based on Kopal exact values plus skin-friction estimates was obtained.

For the body-alone models, the flat-bottom D-body yielded the highest value for $(L/D)_{max}$ of 3.62. For the body-wing models, the highest value for $(L/D)_{max}$ was 3.95, obtained for the flat-bottom D-body with the wing on the bottom. Nose blunting $\left(\frac{\text{Nose radius}}{\text{Base radius}} = 0.0555\right)$ resulted in small losses in $(L/D)_{max}$ for the body-wing configurations, but significant losses were obtained for the body-alone models.

All models were longitudinally and directionally stable about a moment center located at 64.2 percent of the sharp-nose body length. The addition of a wing generally resulted in providing increments of positive dihedral effect on all models at the higher angles of attack. The directional stability either remained unaffected or decreased because of the addition of the wing. At the optimum angles of attack (maximum lift-drag ratios), the flat-top D-body configurations had better lateral stability characteristics than the flat-bottom configurations.

INTRODUCTION

Increased interest in hypersonic cruise and lifting reentry vehicles has led to systematic studies of various body, wing, and body-wing configurations. Of prime interest

in the investigations have been the effects of geometrical variations on the hypersonic efficiency of these configurations. For example, the aerodynamic performance of wings having varying thicknesses and aspect ratios is reported in reference 1, and the effects of body cross-sectional shape are presented in reference 2. Results of investigations on half-cone delta-wing configurations at Mach numbers of 6.86 and 20 are reported in references 3 and 4, respectively. In these two references, effects of the volume parameter and body-wing interference on the maximum lift-drag ratios are included. In references 5 and 6, the major theoretical and experimental results of these and related investigations are summarized.

The purpose of the present investigation was to provide hypersonic data on a family of configurations having maximum lift-drag ratios from 3 to 4. The two basic body shapes tested were a circular cone having a 5° semivertex angle and a 5° half-cone combined with a rectangular pyramid to form a body having a D-shape cross section. The body-wing configurations consisted of these bodies in conjunction with a flat-plate delta wing having a sweep angle of 83.3°. Longitudinal and lateral directional stability characteristics were obtained at a Mach number of 6.83 and a Reynolds number of 1.45×10^6 based on model length. Additional longitudinal stability data were obtained on the circular cone for Reynolds numbers from 0.76×10^6 to 3.00×10^6. Forces and moments were measured by a strain-gage balance for angles of attack from 0° to 15°.

SYMBOLS

b	model span
C	temperature-viscosity proportionality constant
C_A	axial-force coefficient, $\frac{\text{Axial force}}{qS}$
C_D	drag coefficient, $\frac{\text{Drag}}{qS}$
$C_{D,0}$	drag coefficient at $\alpha = 0^{\circ}$
C_F	average skin-friction coefficient, $\frac{\text{Friction drag}}{qS}$
C_L	lift coefficient, $\frac{\text{Lift}}{qS}$
C_l	rolling-moment coefficient, $\frac{\text{Rolling moment}}{qS2r_b}$

$C_{l_\beta} = (\Delta C_l)/(\Delta\beta)_{\beta=0^o,-5^o}$ per deg

C_m pitching-moment coefficient, $\frac{\text{Pitching moment}}{qSl}$

C_N normal-force coefficient, $\frac{\text{Normal force}}{qS}$

C_n yawing-moment coefficient, $\frac{\text{Yawing moment}}{qS2r_b}$

$C_{n_\beta} = (\Delta C_n)/(\Delta\beta)_{\beta=0^o,-5^o}$ per deg

C_Y side-force coefficient, $\frac{\text{Side force}}{qS}$

$C_{Y_\beta} = (\Delta C_Y)/(\Delta\beta)_{\beta=0^o,-5^o}$ per deg

L/D lift-drag ratio

l model reference length

M free-stream Mach number

FB flat-bottom orientation

FT flat-top orientation

q free-stream dynamic pressure

R_l free-stream Reynolds number based on model length

r_n nose radius

r_b base radius

S model planform area

S_c cone model surface area excluding base area

t body thickness

V	model volume (excluding wing)
$V^{2/3}/S$	volume parameter (sharp-nose models)
X,Y,Z	Cartesian body axes
x	distance along center line measured from model nose apex
X_s, Y_s, Z_s	stability axes
X_w, Y_w, Z_w	wind axes
α	angle of attack referenced to model center line
β	angle of sideslip referenced to model center line
θ_c	cone semivertex angle
θ_p	pyramid vertex angle, vertical plane
Λ	wing sweep angle

Subscripts:

mc	moment center
max	maximum
opt	optimum, at maximum L/D

A prime (') denotes a quantity based on local conditions.

APPARATUS AND MODELS

The investigation was conducted in the Langley 11-inch hypersonic tunnel, which is of a blowdown type. A two-dimensional, contoured nozzle fabricated from invar produces a Mach number slightly under 7. To avoid liquefaction, dry air is passed through an electrically heated bundle of Nichrome tubes before entering the tunnel stagnation chamber.

A more detailed description of this facility as well as typical nozzle calibrations may be found in references 7 and 8.

Stagnation temperature was measured by a chromel-alumel thermocouple and the output was recorded on a strip-chart potentiometer. Stagnation pressure was read from a Bourdon gage. The angle of attack was determined optically by reflecting a light beam off a small prism which was embedded in the model surface. This reflected light fell on a screen which was calibrated for the selected angles of attack. Model forces and moments were measured by a water-cooled strain-gage balance having a six-component capability. Strip-chart potentiometers were used for recording balance outputs. A cylindrical windshield was employed to protect the balance from the airstream. Model base pressures were obtained by means of a 3/16-inch (outside diameter) stainless-steel tube connected to a 1.0-psia transducer (6894 N/m^2), which was located just outside the tunnel test section.

The five models tested in this investigation were machined from stainless steel. Photographs of the blunt-nose models and model details are presented in figures 1 and 2, respectively. The body-alone models consisted of a right circular cone having a 5^o semivertex angle (model 1) and a 5^o half-cone in combination with a rectangular pyramid having a vertex angle of 3.56^o in the vertical plane (model 2). Models 3, 4, and 5 incorporated a flat-plate delta wing which had a sweep angle of 83.3^o, a thickness—root-chord ratio of 0.0016, and blunt leading edges. Both models 3 and 4 had the same D-shape cross section as model 2, but a wing was added for these models. For model 3, the wing was alined on the model center line, while for model 4, the wing was mounted flush with the bottom of the body. Thus the wing of model 4 was inclined 3.56^o to the flow when the model was at 0^o angle of attack. The models were tested with sharp and blunt noses. For the blunt-nose conical models, the ratio of nose radius to base radius was 0.0555; the D-body models were cut off at the same longitudinal station as the conical models, and therefore required fairing of the nose over the pyramidal portion.

TESTS AND DATA ACCURACY

The investigation was conducted at a Mach number of 6.83 and an average Reynolds number of 1.45×10^6 based on the model length. Average stagnation pressure and temperature were 13.9 atmospheres absolute $\left(1.4 \times 10^6 \text{ N}/\text{m}^2\right)$ and 1110^o R (617^o K), respectively. Longitudinal force and moment data were obtained over an angle-of-attack range from 0^o to 15^o. Lateral directional data were obtained at a sideslip angle of -5^o over an angle-of-attack range from 0^o to 12^o. For the D-body models 2, 3, and 4, tests were made in the flat-top and flat-bottom orientations. Additional tests were performed on the sharp-nose cone model at 0^o sideslip over a stagnation-pressure range from 7 to

28.6 atmospheres absolute. The corresponding Reynolds number ranged from 0.76×10^6 to 3.00×10^6.

The longitudinal stability characteristics presented herein are based on the body-axis and stability-axis systems, while the lateral directional characteristics are based on the body-axis system. (See fig. 3.) The moment center for the sharp- and blunt-nose models was located on the center line at a point 64.2 percent of the model reference length as measured from the apex of the sharp-nose model. The center line was defined as the axis of the conical portion of each model and was used for the 0^o reference line for angle of attack and angle of sideslip on all models. The axial-force coefficients were adjusted by correcting the measured base pressure to free-stream pressure.

An estimate of balance maximum error is based on 0.5 percent of the maximum design load of each component. These force and moment errors, expressed in coefficient form, are as follows:

Estimates of errors in	Models 1 and 2	Models 3, 4, and 5
C_N	±0.0023	±0.0017
C_A	±0.0007	±0.0005
C_m	±0.00023	±0.00017
C_l	±0.0003	±0.00026
C_n	±0.0004	±0.0003
C_Y	±0.0007	±0.0004

The maximum error in $(L/D)_{max}$ was calculated to be ±0.20, which includes an angle-of-attack error of $\pm 0.2^o$ and the error in base pressure taken at 0.5 percent of transducer maximum output. The Mach number is estimated to be accurate within ±0.04, and the sideslip angle, within $\pm 0.10^o$.

RESULTS AND DISCUSSION

Presentation of Results

The effects of Reynolds number variation on the longitudinal aerodynamic characteristics of the cone model 1 are presented in figures 4 and 5. The longitudinal aerodynamic characteristics for the body-alone models are shown in figures 6(a) and 6(b) and for the body-wing models in figures 6(c) to 6(e) for a constant Reynolds number of 1.45×10^6. For the D-body models, data are presented for positive and negative angles of attack, which correspond to flat-bottom and flat-top orientations, respectively. In

figure 7, a summary of the longitudinal aerodynamic performances of the five models is presented. Drag polars (not presented) were utilized in determining the values of the parameters shown in figure 7. The lateral directional derivatives for the five models having nose bluntness are shown in figure 8. In figure 9, the effects of wing addition on the lateral directional derivatives are presented. A summary of these derivatives taken at the optimum angle of attack for each configuration is presented in figure 10.

Reynolds Number Variation

The longitudinal aerodynamic characteristics of the sharp 5° cone model 1 are presented in figure 4 for a Reynolds number range from 0.76×10^6 to 3.00×10^6. Also included in the figure is Newtonian theory, as well as Newtonian theory plus the laminar skin-friction coefficient C_F for the minimum and maximum test Reynolds numbers. Values of C_F were calculated from the following equation of reference 9:

$$C_F = \frac{1.328\sqrt{C}}{\sqrt{R_l'}} \frac{2\sqrt{3}}{3} \frac{S_c}{S} \frac{q'}{q}$$

This equation, which assumes a laminar boundary layer, incorporates the transformation constant $2\sqrt{3}/3$. (See ref. 10.) For the test conditions of this investigation, a value of 0.86 was used for C. The skin-friction coefficients were calculated at 0° angle of attack and assumed constant throughout the angle-of-attack range.

Generally good agreement is obtained between Newtonian theory and experiment for the normal-force coefficients and the pitching-moment coefficients for angles of attack up to about 7°. The expected differences existing between the measured axial-force coefficients and the values predicted by Newtonian theory are mainly attributable to skin friction. The differences increase with decreasing Reynolds number. Inclusion of calculated values of C_F with Newtonian theory results in a significant improvement in predicting axial-force and drag coefficients. Predicted values of L/D based on Newtonian theory plus C_F are in good agreement with the experimental values at angles of attack from about 6° to 15°; at lower angles of attack, theory greatly overestimates the experimental values.

In figure 5, the parameters $(L/D)_{max}$ and $C_{D,0}$ are presented as functions of Reynolds number for the 5° cone model 1. The measured values of $(L/D)_{max}$ are in good agreement with predictions based on Newtonian theory plus C_F, whereas agreement only in the trends of $C_{D,0}$ is obtained. However, use of the Kopal values for the pressure drag (tabulated in ref. 11) improves the agreement between theoretical and experimental values of $C_{D,0}$ over the range of Reynolds numbers investigated.

Longitudinal Aerodynamic Characteristics

Body-alone models.- For the sharp-nose models, the summary chart of figure 7 indicates a value of $(L/D)_{max}$ of 3.62 for the flat-bottom D-body model, as compared with values of 3.25 and 3.30 obtained for the cone model and the flat-top D-body model, respectively. The superiority of the flat-bottom orientation is consistent with the results reported in references 5 and 6. Slightly better performance of the flat-top D-body model as compared with the cone model may be attributed to the lower values of volume parameter and thickness ratio of the D-body. The pitching-moment coefficients in figures 6(a) and 6(b) indicate positive stability for the cone model and the model with the flat-bottom D-body. The flat-bottom D-bodies show a somewhat higher level of stability at $(L/D)_{max}$ than the cone.

Nose bluntness of the body-alone models results in significant losses in $(L/D)_{max}$. The D-body models experience a loss of about 0.40, which is about twice that obtained for the cone model. The greater sensitivity of the more slender D-bodies to nose blunting is also observed from the axial-force coefficients, as shown in figures 6(a) and 6(b). Small increases in optimum angle of attack (no greater than 0.3^{o}) with attendant increases in $C_{L,opt}$ result from nose blunting. Removal of the forward lifting area by blunting causes an increase in positive stability, as shown in figures 6(a) and 6(b).

Body-wing models.- Addition of the wings to the sharp-nose bodies increases the maximum lift-drag ratio. (See fig. 7.) Again the flat-bottom models are superior to the flat-top models and the cone model. The highest value for $(L/D)_{max}$ was 3.95, obtained for model 4 where the wing was mounted flush with the bottom surface of the model. This value compares with values of 3.75 and 3.65 measured for the flat-bottom and flat-top orientations of model 3. A value for $(L/D)_{max}$ of 3.55 was measured for the flat-top orientation of model 4, an indication that favorable body-wing interference effects are negligible. This result agrees with trends of reference 3 which show that favorable interference effects disappear for wing sweep angles greater than about 82^{o} for the Mach number and Reynolds number of the present investigation.

In general, nose bluntness effects on the body-wing configurations are not as pronounced as those obtained on the body-alone models. Losses in $(L/D)_{max}$ ranged from 0.07 to 0.15 for the body-wing models 3 and 4. The blunt-nose version of model 5, however, produces a value of $(L/D)_{max}$ slightly higher than that measured for the sharp-nose version. This difference of 0.05 is well within the estimated accuracy for $(L/D)_{max}$. Nose blunting has little effect on axial-force coefficients (figs. 6(c) to 6(e)) or optimum angle of attack (fig. 7). Some improvement in longitudinal stability is obtained, as shown in figures 6(c) to 6(e).

Lateral Directional Characteristics

The lateral directional derivatives for the blunt-nose body-alone models 1 and 2 are presented in figure 8(a). The cone and the flat-bottom D-body have about the same level of directional stability $\left(C_{n_\beta}\right)$ throughout the angle-of-attack range. The flat-top D-body, however, shows a significant increase in directional stability as the angle of attack is increased beyond 4^o; in hand with this trend, the side-force derivative also increases negatively with angle of attack. For the cone, the corresponding side-force parameter increases slightly with angle of attack as predicted by Newtonian force estimates in reference 12. Whereas the flat-bottom D-body has negative dihedral effect, for the flat-top orientation the effect is positive; the cone is neutrally stable about the assumed moment center.

In figure 8(b), the lateral directional derivatives are presented for the body-wing models 3, 4, and 5. All models are directionally stable over the angle-of-attack range. The sizable decrease in C_{n_β} with angle of attack is noted for the flat-bottom orientation of model 4 and is attributed to shielding effects of the wing; for the flap-top orientation of model 4, C_{n_β} increases for angles of attack greater than about 5^o. This trend is due to the fact that the entire fuselage is exposed to the flow at angles of attack greater than 3.5^o. The flat-top and flat-bottom orientations of the midwing model (model 3) have about the same level of directional stability throughout the angle-of-attack range. Models 3 and 4 in the flat-top orientation and model 5 are laterally stable. It is clear that mutual interference effects with the wing in the top position produce highly stabilizing pressures along the windward wing and flat sides of the body. The flat-bottom versions of models 3 and 4 are laterally unstable at low angles of attack but stable at angles of attack greater than 2^o and 8^o, respectively. Little variation in the side-force derivative is obtained for all the body-wing models except model 4 in the flat-top orientation, for which the magnitude of C_{Y_β} increases significantly with angle of attack.

In figure 9, the effects of addition of the wing to the cone and D-bodies on the lateral directional derivatives are shown for the blunt-nose models. In order to make this comparison, adjustments were made to the derivatives of the body-alone models by using the wing planform area for the reference area. For the conical models (fig. 9(a)), wing addition results in increasing positive dihedral effect with angle of attack. Small decreases in the directional stability and the side-force derivative are obtained at the higher angles of attack.

Wing addition to the flat-top D-body models (fig. 9(b)) results in large increments of positive dihedral for model 4 throughout the angle-of-attack range because of the location of the wing. The midwing configuration (model 3) shows a more moderate increase in lateral stability which occurs only at angles of attack greater than about 4^o; addition of the wing to the flat-top configuration results in some loss in directional stability and the

side-force derivative. Very small increases in directional stability are noted for model 4; however, significant increases which are obtained in the side-force derivative suggest center-of-pressure variation for this model.

For the flat-bottom D-body models (fig. 9(c)), adding the wing again results in increments of positive dihedral effect, the magnitudes of which become significantly larger as angle of attack increases for model 3; this trend is also true for model 4 at angles of attack greater than 6°. At the lower angles of attack, the incremental dihedral effect is negative. A decrease in directional stability is noted for model 4 at angles of attack greater than 4°; it is primarily caused by the large amount of shielding by the wing. Together with this trend, decreases in the side-force derivative are obtained. The effects of wing addition on the directional stability and the side-force derivatives of the midwing model in the flat-bottom orientation are generally negligible.

Aside from the effects of wing addition, figure 9 also shows that the pyramidal portion of the model is aerodynamically more effective than the conical surface. This fact is evident from the lateral stability results for both flat-top and flat-bottom orientations of the body-alone model 2 when compared with model 1 at 0° angle of attack. Also, losses in directional stability and side-force derivative were previously noted for model 3 in the flat-top orientation as compared with the flat-bottom orientation at the higher angles of attack. This result reflects the effect of shielding the upper pyramidal portion of the model by the wing. For the flat-bottom version of model 3, shielding the upper conical surface results in only small changes in directional stability and side-force parameter.

A summary of the lateral and directional derivatives at the optimum angles of attack (fig. 7) is presented in figure 10 for all blunt-nose models including the D-body models in the flat-top orientation. All the configurations are directionally stable, but the flat-top models indicate somewhat greater stability than their flat-bottom counterparts. The apparent loss in directional stability associated with addition of the wing is primarily a result of the difference in reference area used in reducing data for the bodies alone and for the body-wing configurations. The trends of C_{Y_β} are compatible with those of C_{n_β}. Lateral stability is obtained for the flat-top orientations of models 2, 3, and 4 and model 5; however, only the midwing model (model 3) of the flat-bottom configurations is stable.

CONCLUSIONS

Wind-tunnel tests of a cone and D-body and body-wing configurations conducted at a Mach number of 6.83 and a Reynolds number of 1.45×10^6 lead to the following conclusions;

1. For the sharp 5° cone, predictions of Newtonian theory plus skin-friction estimates showed good agreement with measured values of the maximum lift-drag ratio $(L/D)_{max}$ over a range of Reynolds numbers from 0.76×10^6 to 3.00×10^6. Very good

agreement between measured values of minimum drag coefficient and predicted values based on Kopal exact values plus skin-friction estimates was obtained.

2. For the body-alone models, the flat-bottom D-body yielded the highest value for $(L/D)_{max}$ of 3.62.

3. For the body-wing models, the highest value for $(L/D)_{max}$ was 3.95, obtained for the flat-bottom D-body with the wing on the bottom.

4. Nose blunting $\left(\frac{\text{Nose radius}}{\text{Base radius}} = 0.0555\right)$ caused small losses in $(L/D)_{max}$ for the body-wing models, but significant losses were obtained for the body-alone models.

5. All models were longitudinally and directionally stable about a moment center located at 64.2 percent of the sharp-nose model length.

6. The addition of a wing generally resulted in providing increments of positive dihedral effect on all models at the higher angles of attack. The directional stability either remained unaffected or decreased because of the addition of the wing.

7. In general, the flat-top D-body models had better lateral stability characteristics than the flat-bottom configurations at the optimum angles of attack.

Langley Research Center,
National Aeronautics and Space Administration,
Langley Station, Hampton, Va., May 4, 1966.

REFERENCES

1. Penland, Jim A.: Maximum Lift-Drag-Ratio Characteristics of Rectangular and Delta Wings at Mach 6.9. NASA TN D-2925, 1965.

2. Whitehead, Allen H., Jr.: Effect of Body Cross Section and Width-Height Ratio on Performance of Bodies and Delta-Wing—Body Combinations at Mach 6.9. NASA TN D-2886, 1966.

3. Fetterman, David E.: Favorable Interference Effects on Maximum Lift-Drag Ratios of Half-Cone Delta-Wing Configurations at Mach 6.86. NASA TN D-2942, 1965.

4. Johnston, Patrick J.; Snyder, Curtis D.; and Witcofski, Robert D.: Maximum Lift-Drag Ratios of Delta-Wing—Half-Cone Combinations at a Mach Number of 20 in Helium. NASA TN D-2762, 1965.

5. Fetterman, David E.; Henderson, Arthur, Jr.; Bertram, Mitchel H.; and Johnston, Patrick J.: Studies Relating to the Attainment of High Lift-Drag Ratios at Hypersonic Speeds. NASA TN D-2956, 1965.

6. Becker, John V.: Studies of High Lift/Drag Ratio Hypersonic Configurations. Proceedings of the 4th Congress of the International Council of the Aeronautical Sciences, Robert R. Dexter, ed., Spartan Books, Inc., 1965, pp. 877-910.

7. McLellan, Charles H.; Williams, Thomas W.; and Bertram, Mitchel H.: Investigation of a Two-Step Nozzle in the Langley 11-Inch Hypersonic Tunnel. NACA TN 2171, 1950.

8. Bertram, Mitchel H.: Exploratory Investigation of Boundary-Layer Transition on a Hollow Cylinder at a Mach Number of 6.9. NACA Rept. 1313, 1957. (Supersedes NACA TN 3546.)

9. Chapman, Dean R.; and Rubesin, Morris W.: Temperature and Velocity Profiles in the Compressible Laminar Boundary Layer With Arbitrary Distribution of Surface Temperature. J. Aeron. Sci., vol. 16, no. 9, Sept. 1949, pp. 547-565.

10. Eckert, Ernst R. G.: Survey on Heat Transfer at High Speeds. ARL 189, U.S. Air Force, Dec. 1961.

11. Sims, Joseph L.: Tables for Supersonic Flow Around Right Circular Cones at Zero Angle of Attack. NASA SP-3004, 1964.

12. Wells, William R.; and Armstrong, William O.: Tables of Aerodynamic Coefficients Obtained From Developed Newtonian Expressions for Complete and Partial Conic and Spheric Bodies at Combined Angles of Attack and Sideslip With Some Comparisons With Hypersonic Experimental Data. NASA TR R-127, 1962.

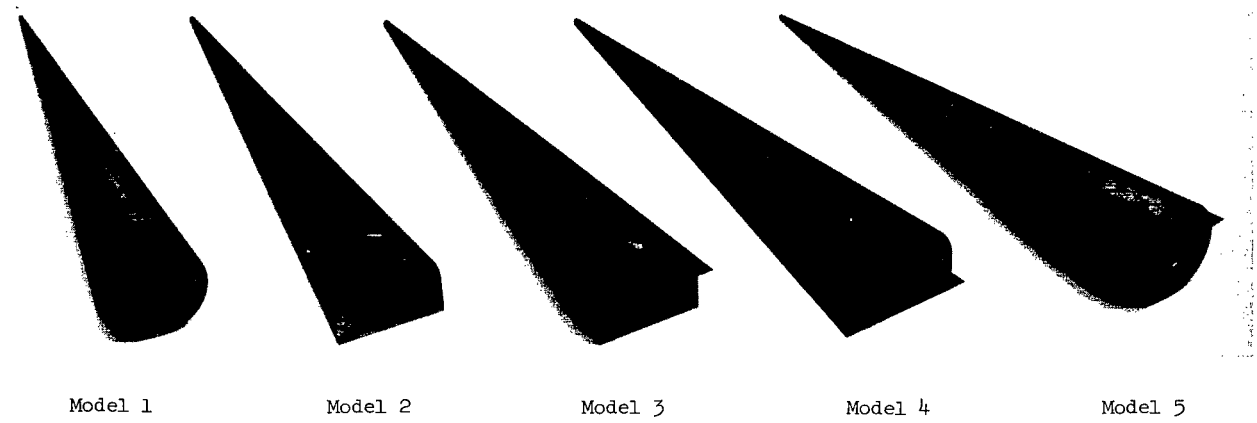

Model 1 Model 2 Model 3 Model 4 Model 5

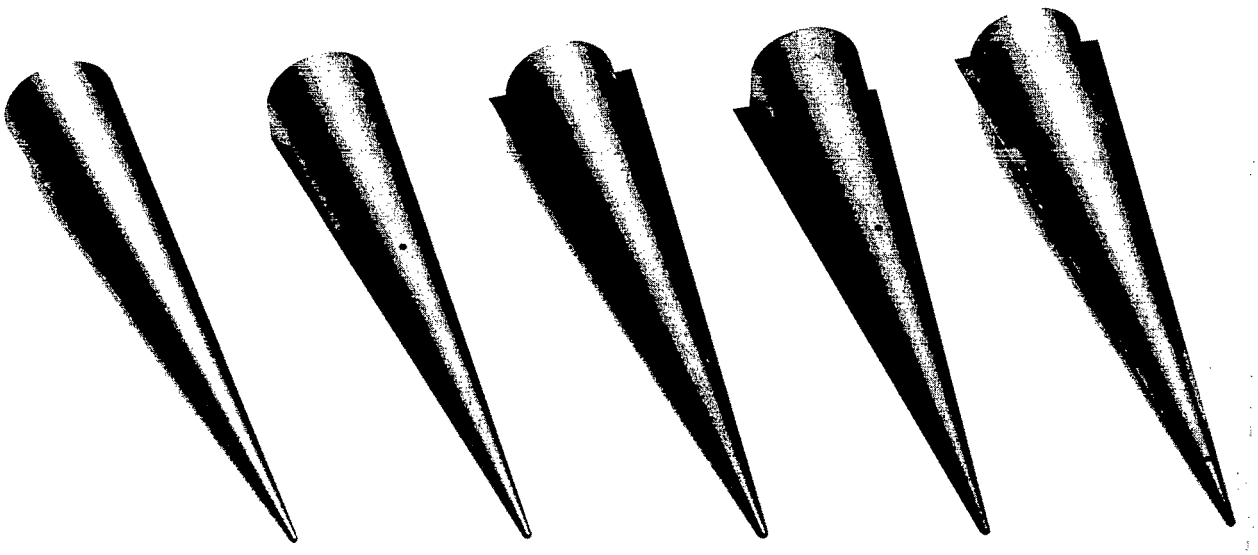

Model 1 Model 2 Model 3 Model 4 Model 5

Figure 1.- Photographs of blunt-nose models.

L-66-1196

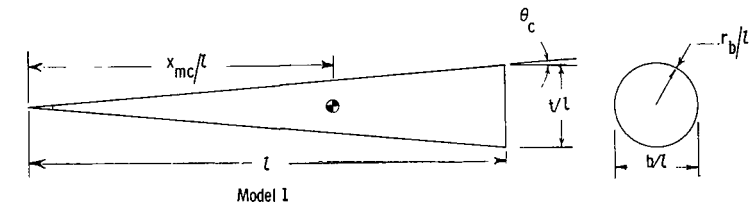

Model 1

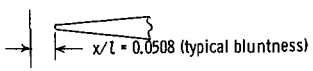

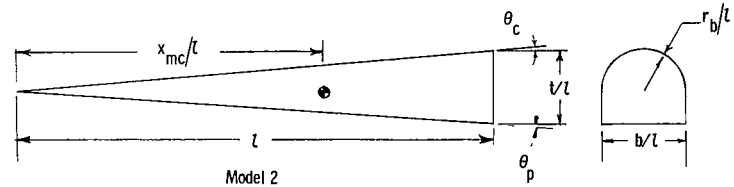

Model 2

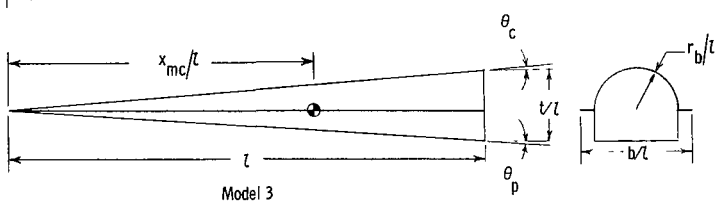

Model 3

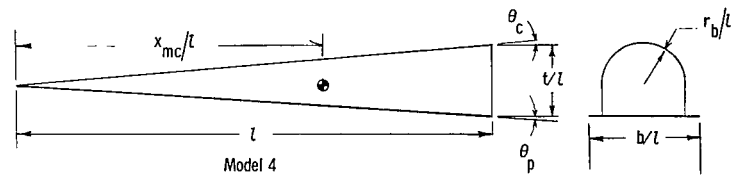

Model 4

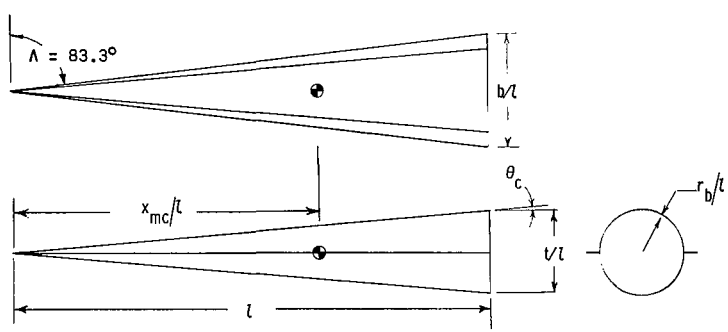

Model 5

Model	$\frac{b}{l}$	l, cm	$\frac{r_b}{l}$	$\frac{x_{mc}}{l}$	$\frac{t}{l}$	θ_c, deg	θ_p, deg	$\frac{V^{2/3}}{S}$	S, cm^2
1	0.1750	25.4	0.0875	0.642	0.1750	5		0.458	56.4
2	.1750	25.4	.0875	.642	.1497	5	3.56	.369	56.4
3	.2333	25.4	.0875	.642	.1497	5	3.56	.277	75.2
4	.2333	25.4	.0875	.642	.1497	5	3.56	.277	75.2
5	.2333	25.4	.0875	.642	.1750	5		.343	75.2

Wing thickness = 0.0016 l

Figure 2.- Details of model dimensions.

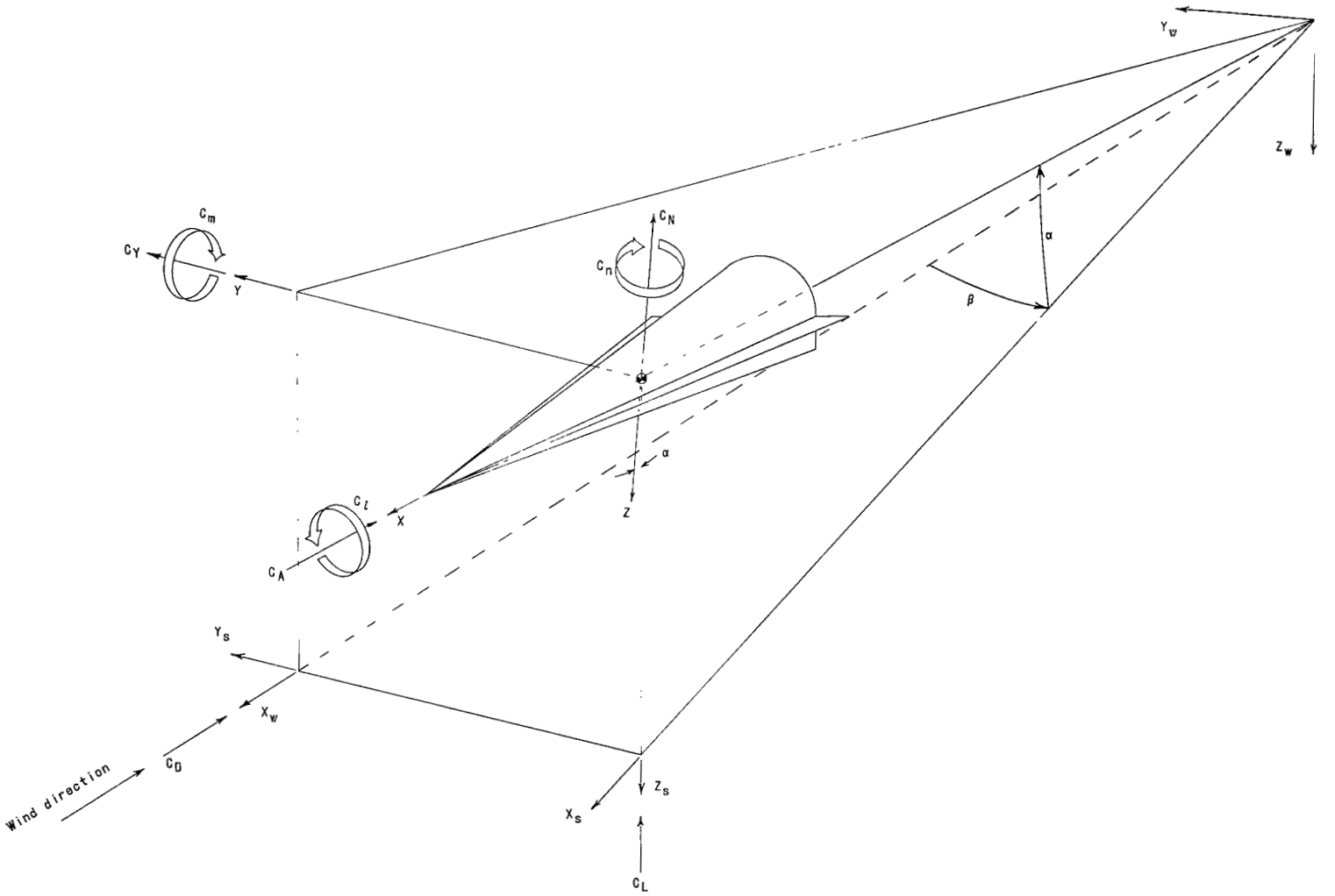

Figure 3.- Axis systems. Arrows indicate positive direction.

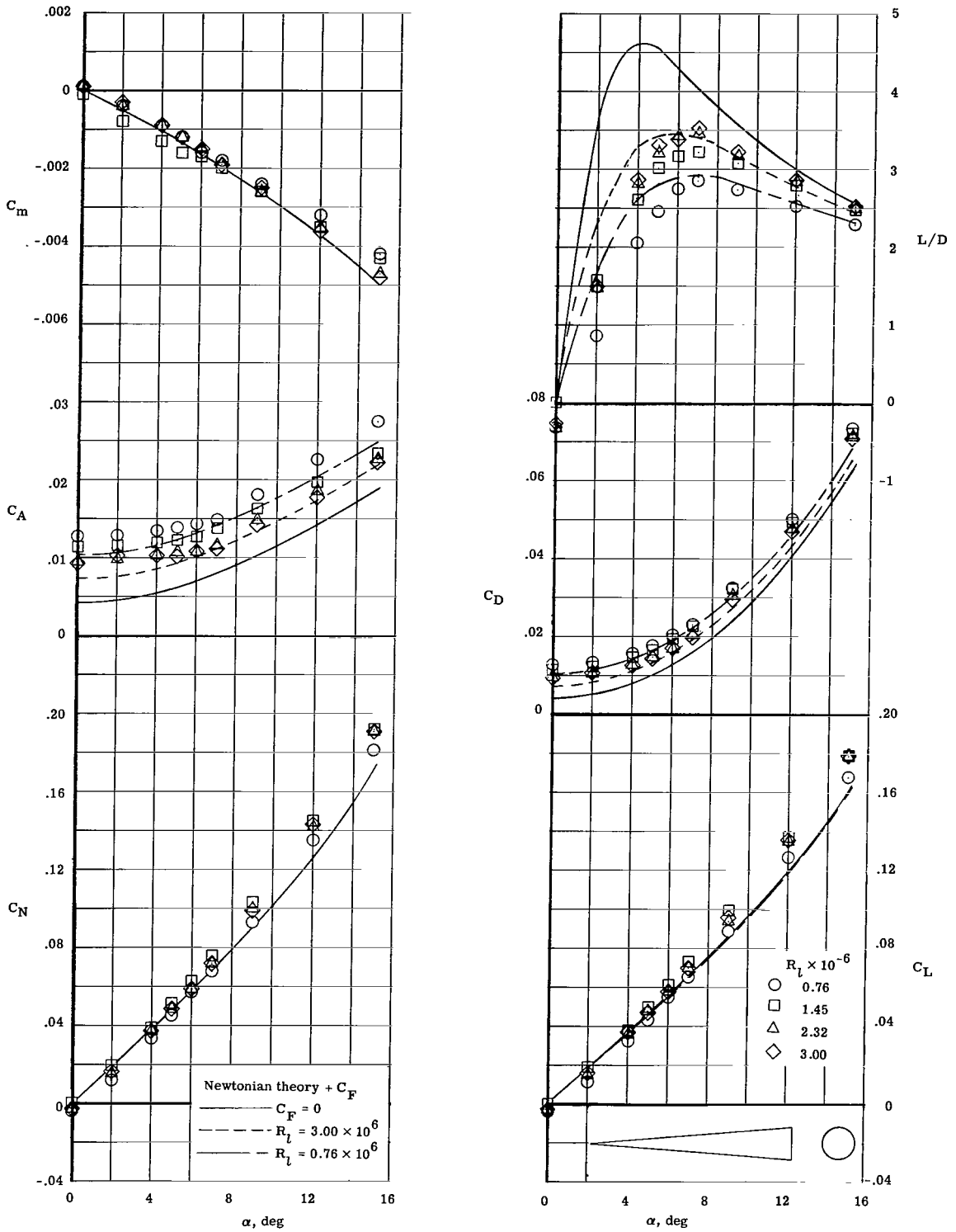

Figure 4.- Longitudinal aerodynamic characteristics of model 1 with varying Reynolds number. $r_n/r_b = 0$.

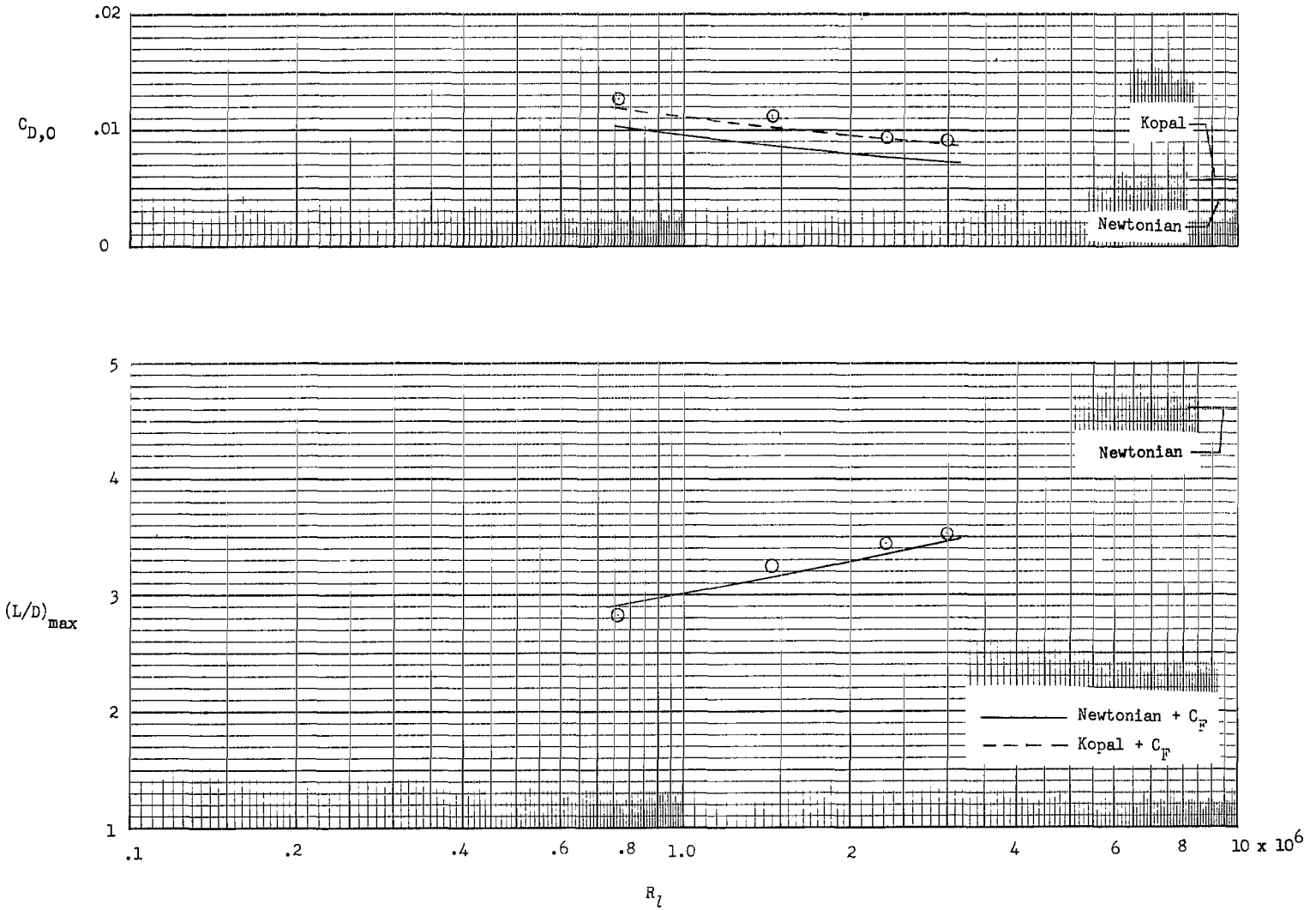

Figure 5.- Effect of Reynolds number on minimum drag and maximum lift-drag ratio for model 1. $r_n/r_b = 0$.

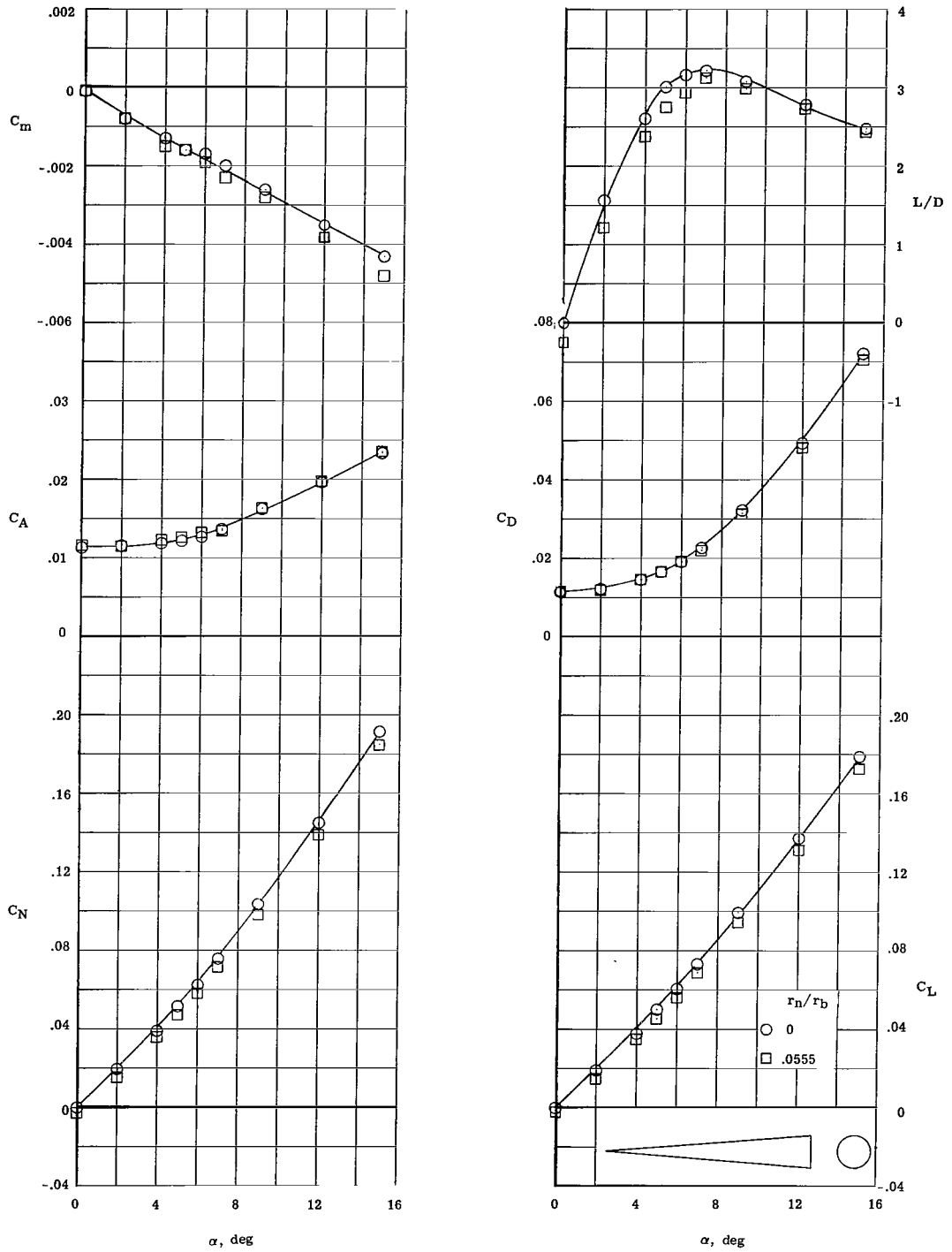

(a) Model 1.

Figure 6.- Longitudinal aerodynamic characteristics. M = 6.83; $R_l = 1.45 \times 10^6$.

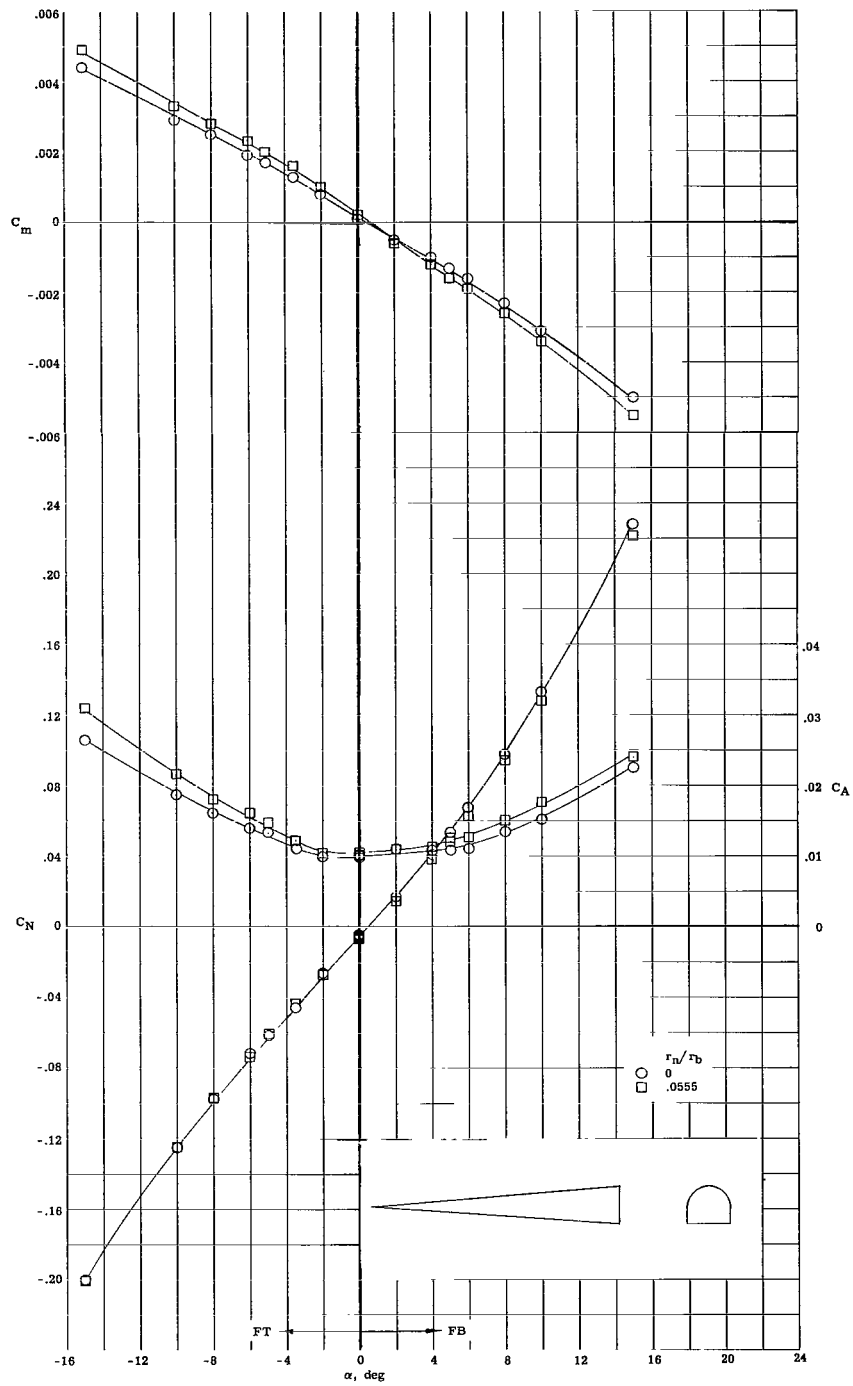

(b) Model 2.

Figure 6.- Continued.

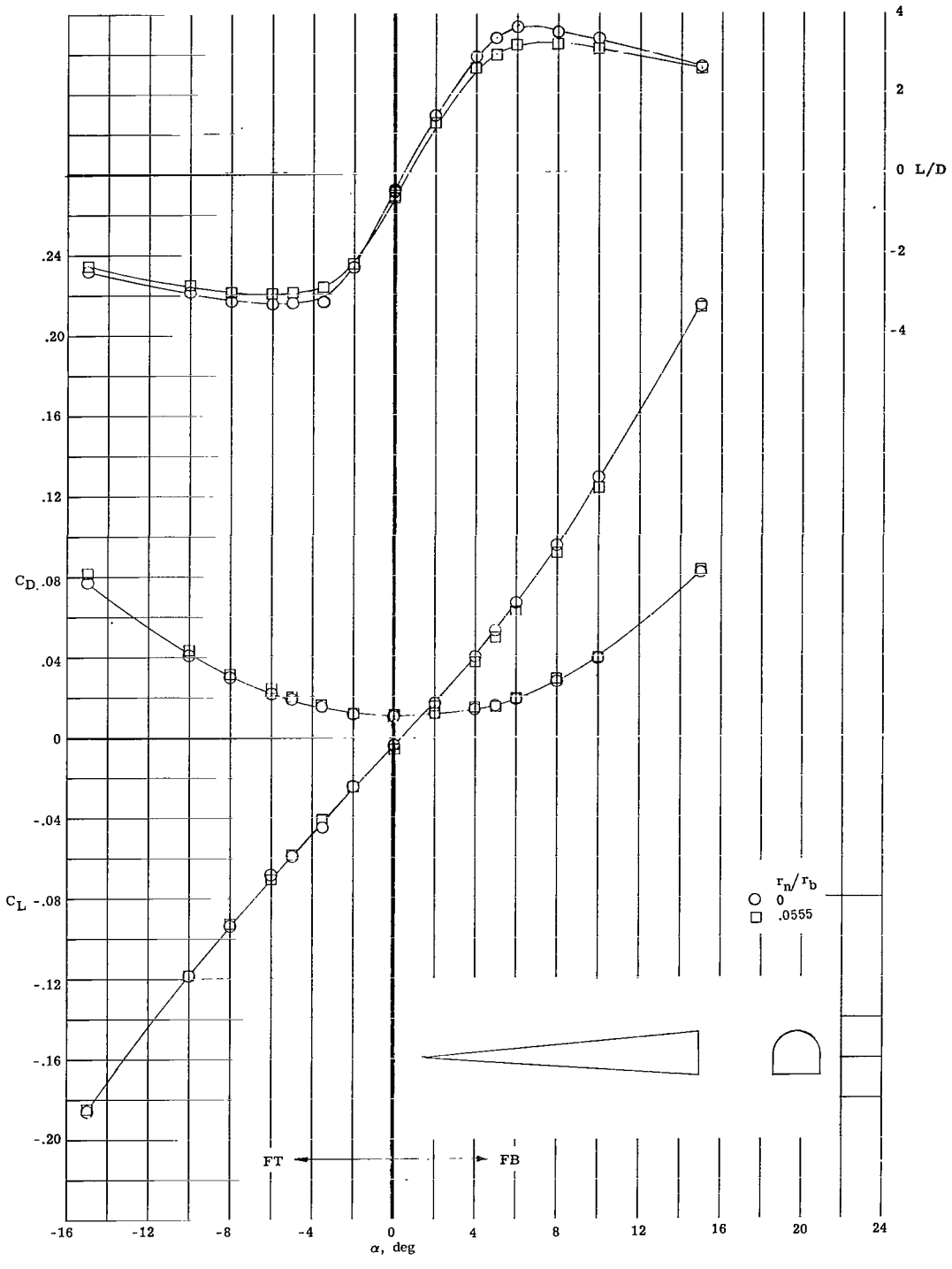

(b) Concluded.

Figure 6.- Continued.

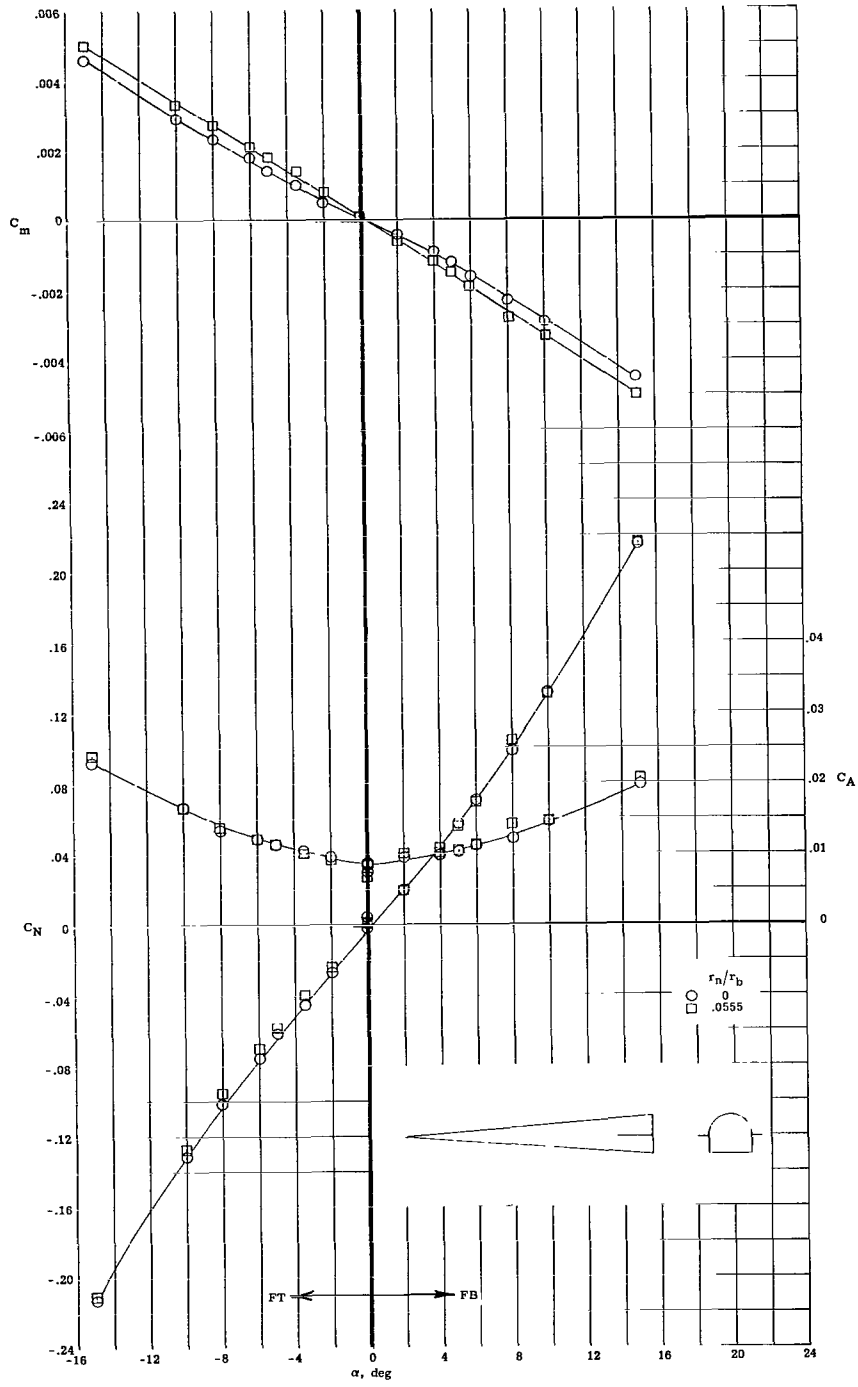

(c) Model 3.

Figure 6.- Continued.

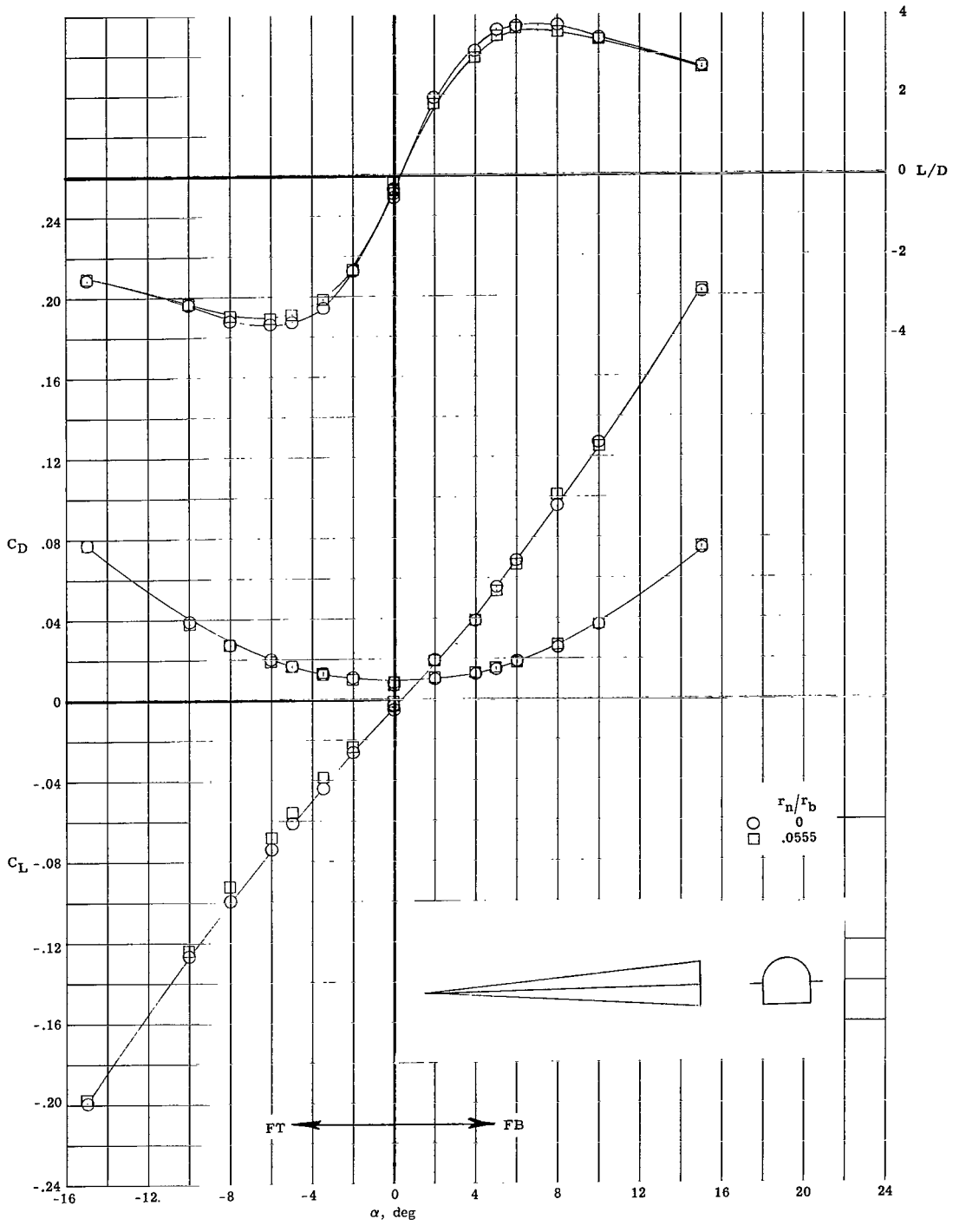

(c) Concluded.

Figure 6.- Continued.

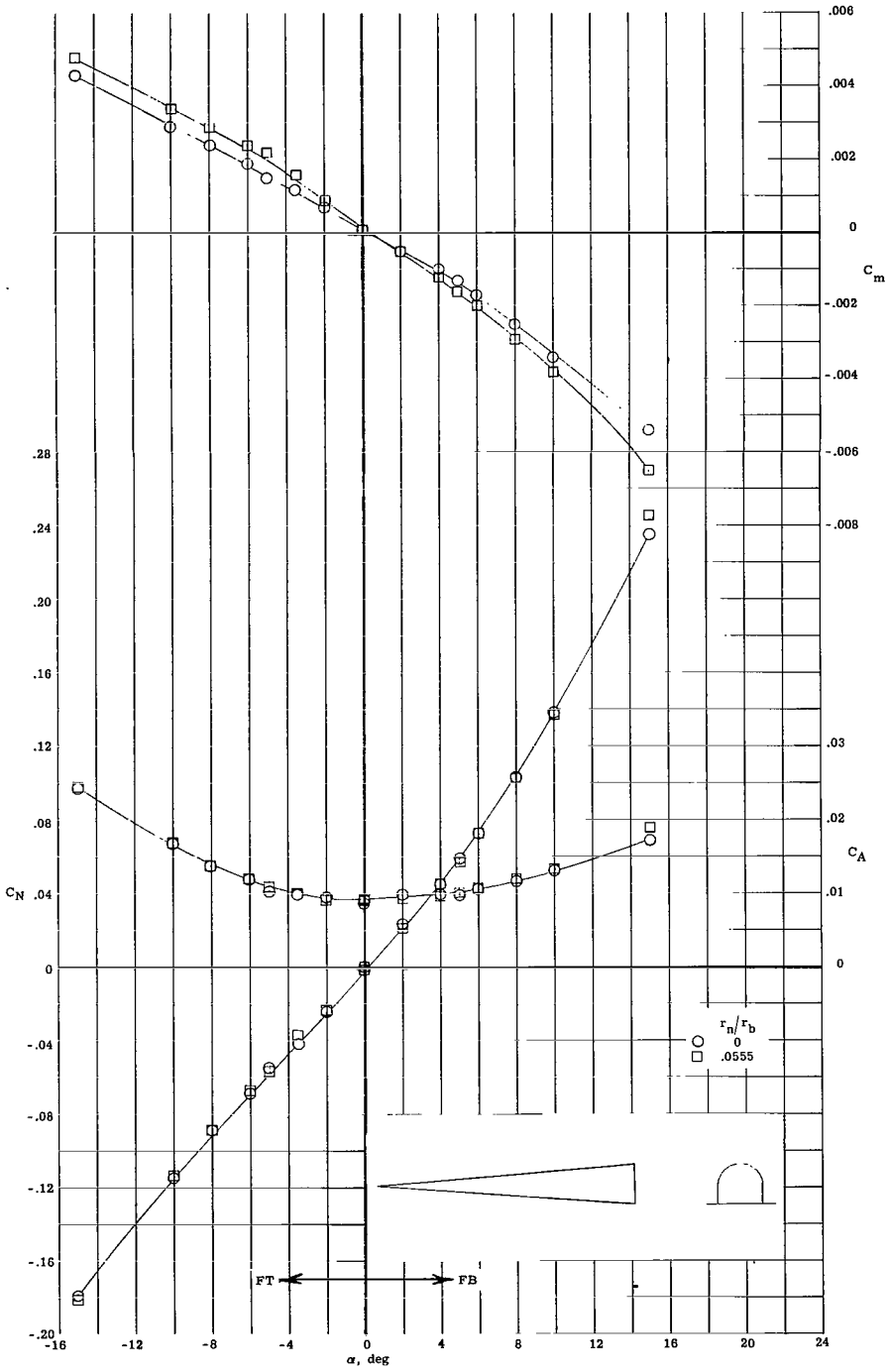

(d) Model 4.

Figure 6.- Continued.

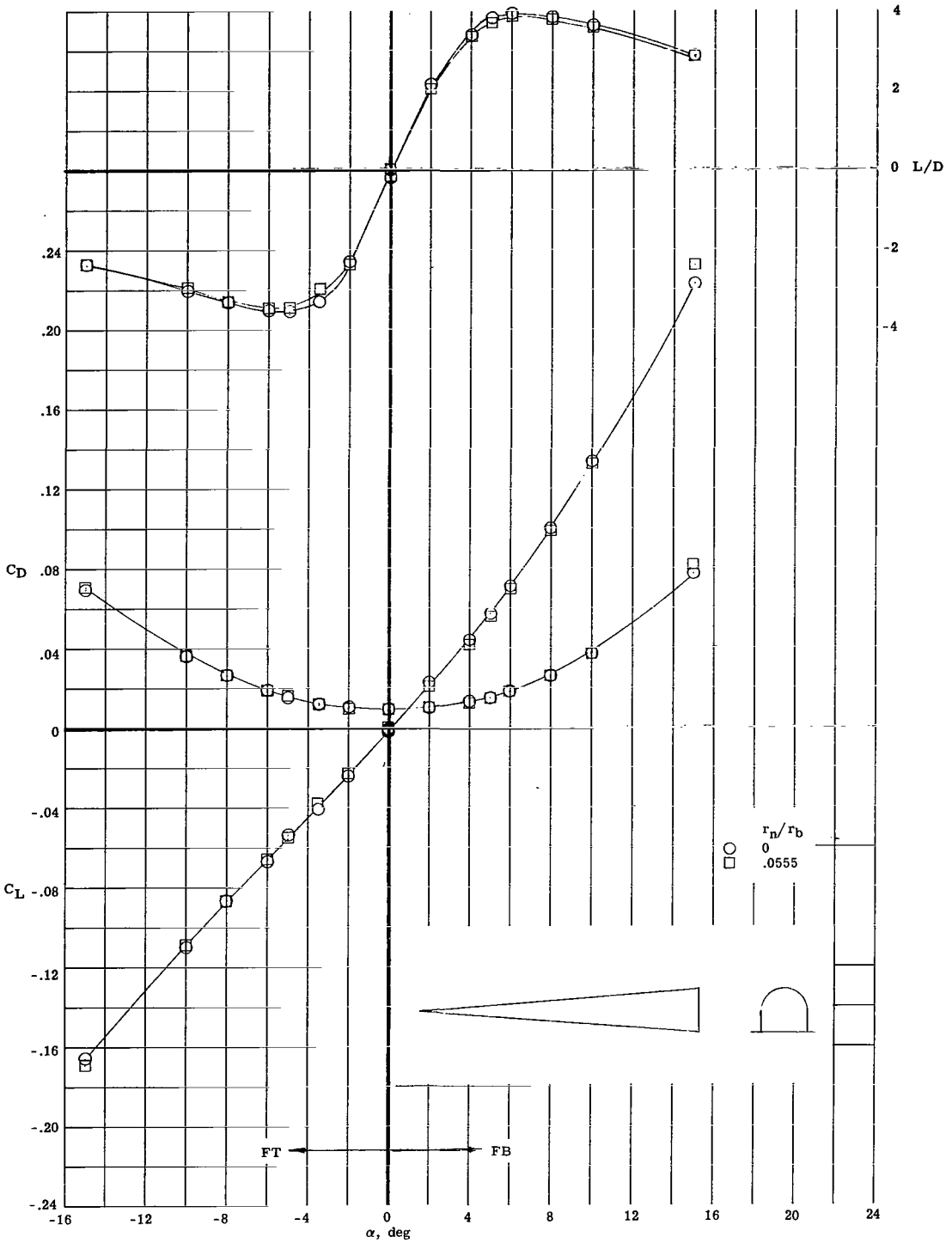

(d) Concluded.

Figure 6.- Continued.

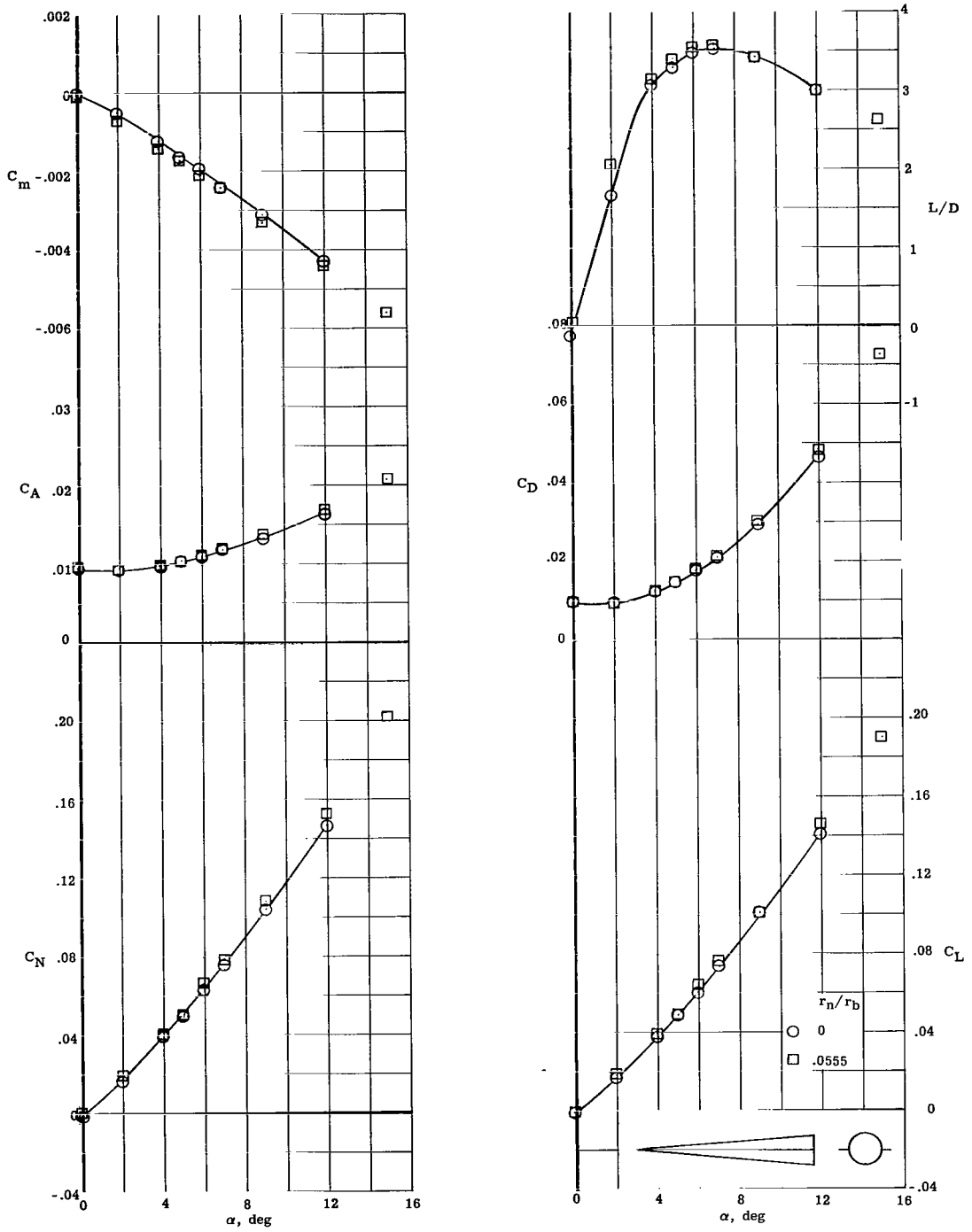

(e) Model 5.

Figure 6.- Concluded.

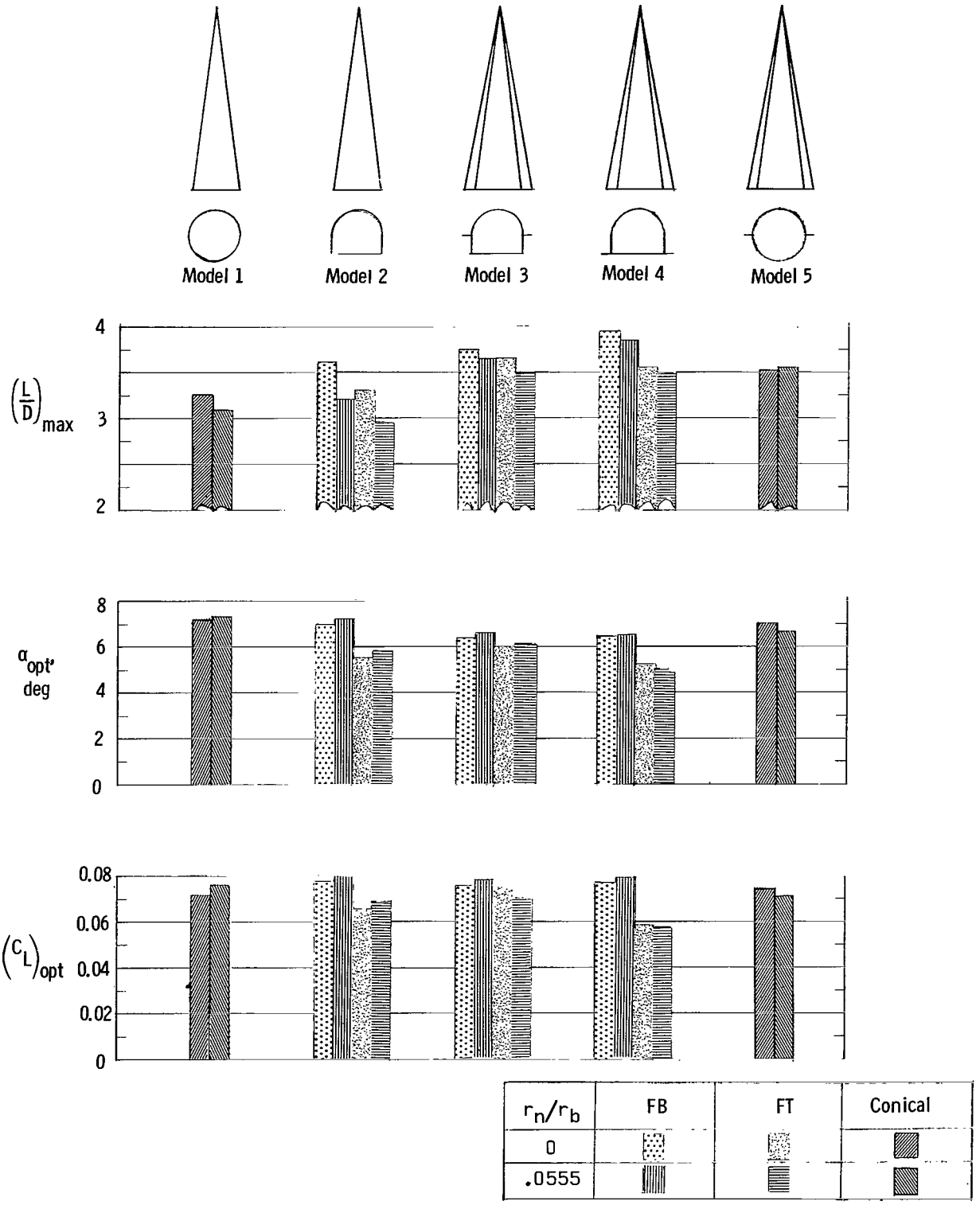

Figure 7.- Summary of longitudinal aerodynamic characteristics. M = 6.83; $R_l = 1.45 \times 10^6$.

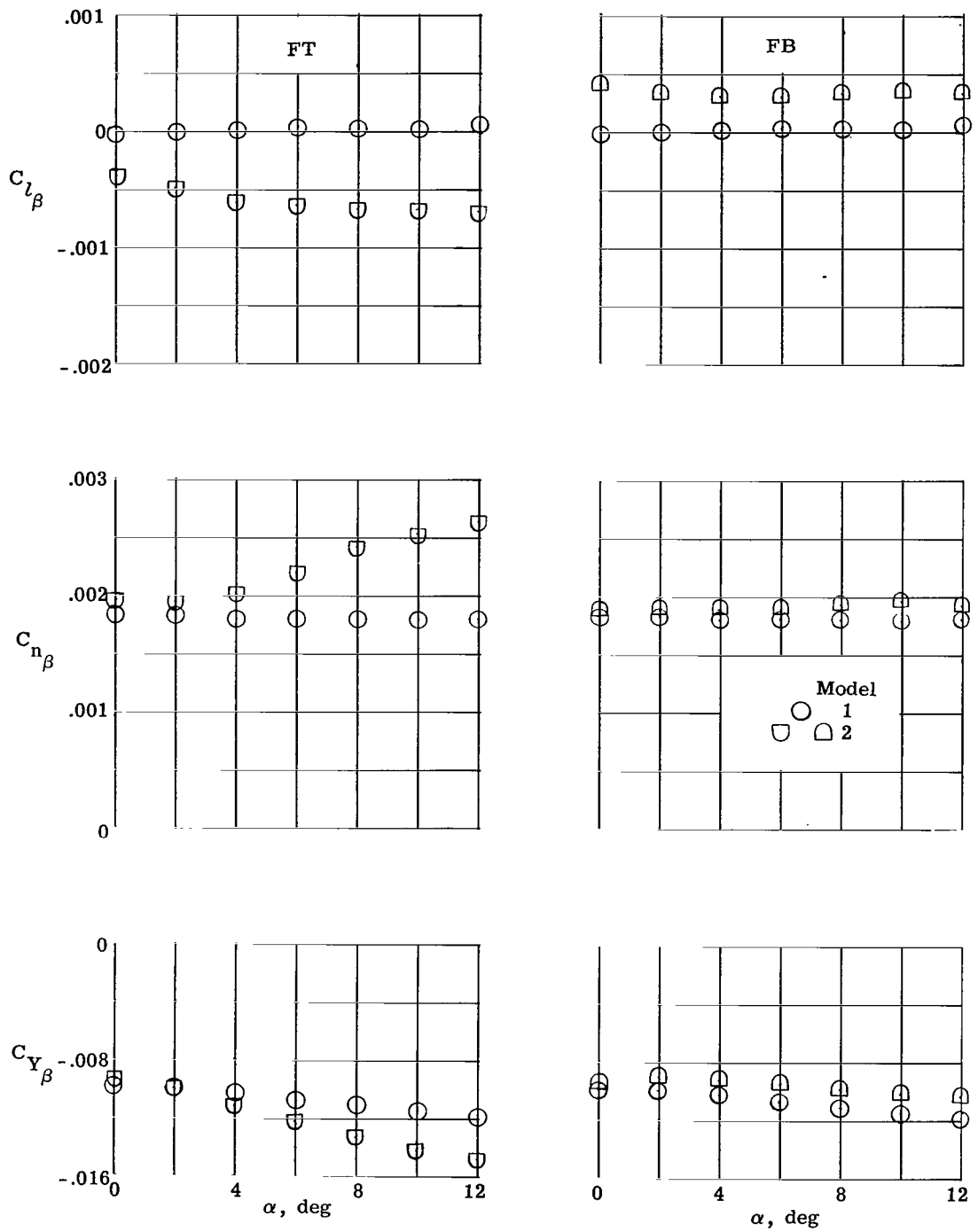

(a) Body-alone models.

Figure 8.- Variation of lateral directional derivatives with angle of attack for blunt-nose models. $r_n/r_b = 0.0555$; $M = 6.83$; $R_\ell = 1.45 \times 10^6$.

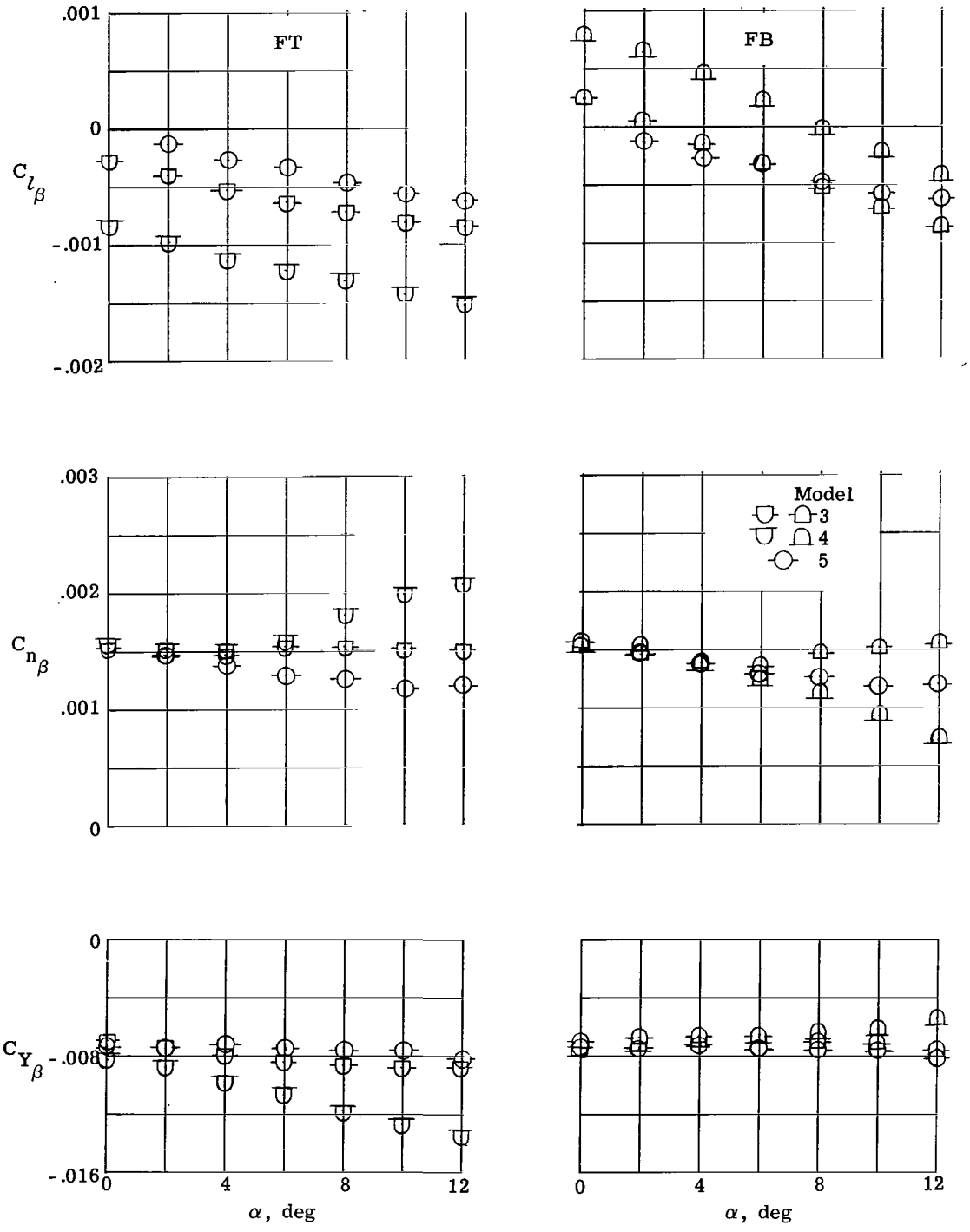

(b) Body-wing models.

Figure 8.- Concluded.

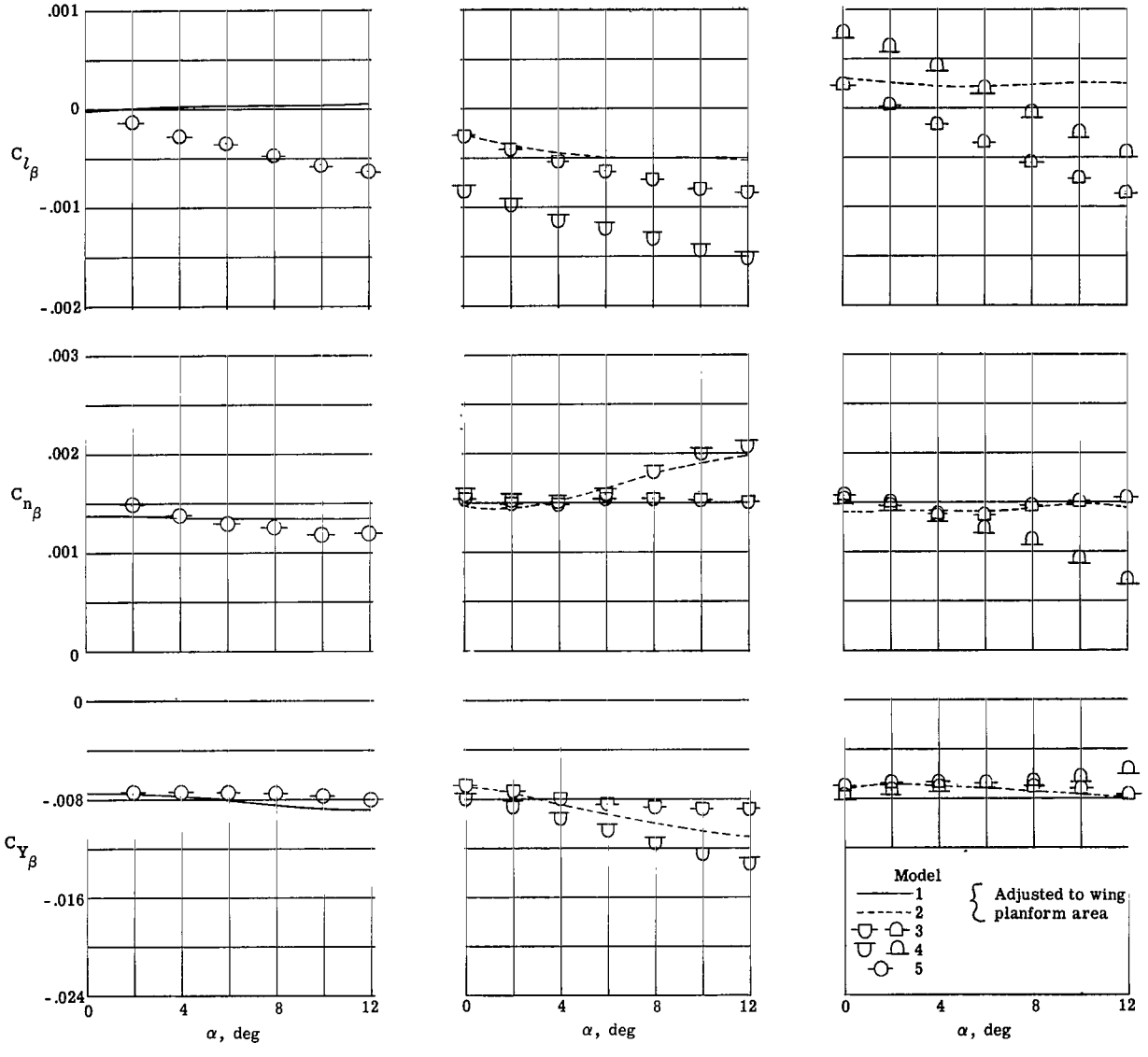

(a) Conical models. (b) Flat-top D-body models. (c) Flat-bottom D-body models.

Figure 9.- Effect of wing addition on lateral directional derivatives. $r_n/r_b = 0.0555$.

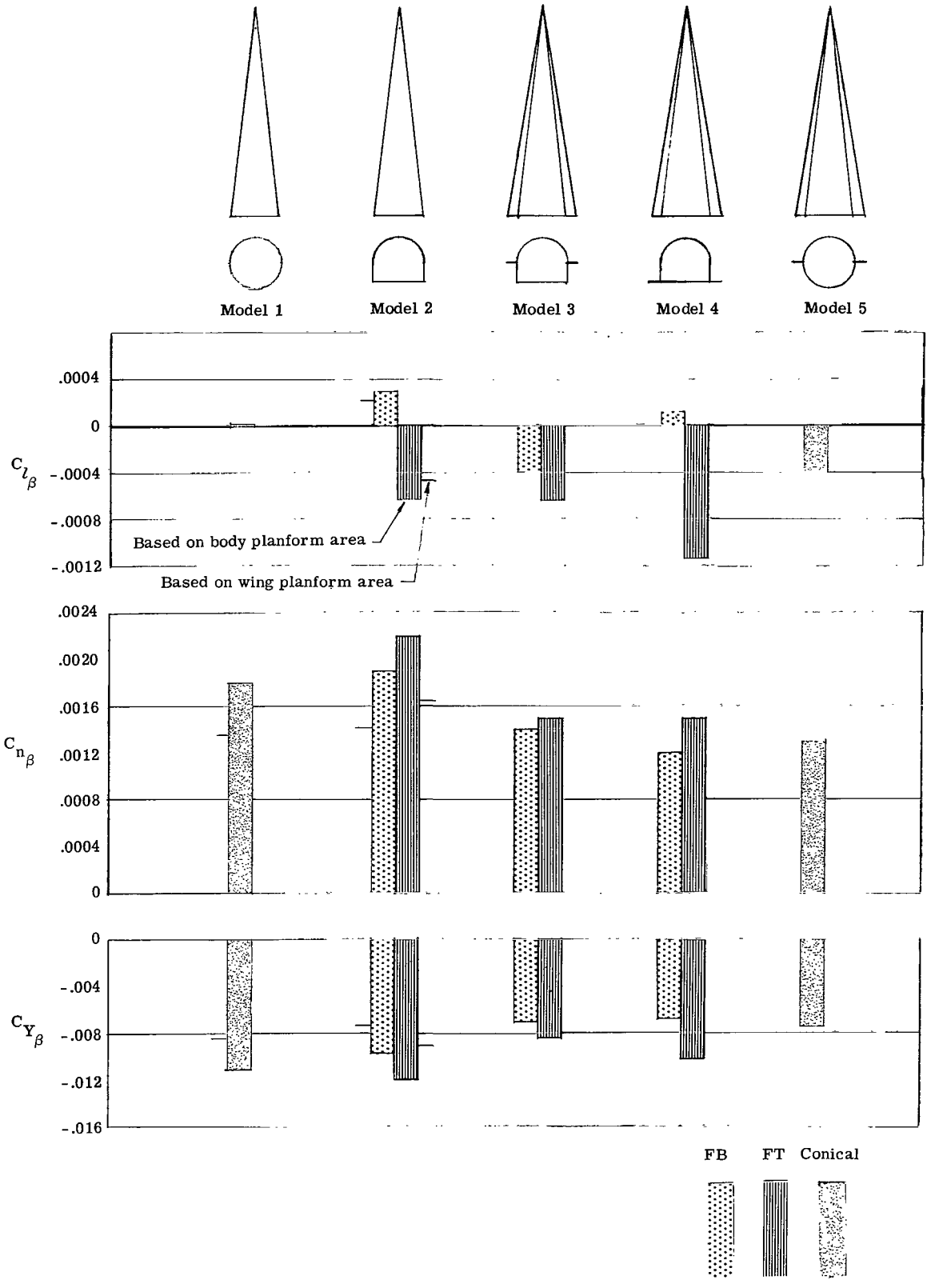

Figure 10.- Summary of lateral directional derivatives at optimum angles of attack. $r_n/r_b = 0.0555$; $R_l = 1.45 \times 10^6$; $M = 6.83$

"The aeronautical and space activities of the United States shall be conducted so as to contribute . . . to the expansion of human knowledge of phenomena in the atmosphere and space. The Administration shall provide for the widest practicable and appropriate dissemination of information concerning its activities and the results thereof."

—NATIONAL AERONAUTICS AND SPACE ACT OF 1958

NASA SCIENTIFIC AND TECHNICAL PUBLICATIONS

TECHNICAL REPORTS: Scientific and technical information considered important, complete, and a lasting contribution to existing knowledge.

TECHNICAL NOTES: Information less broad in scope but nevertheless of importance as a contribution to existing knowledge.

TECHNICAL MEMORANDUMS: Information receiving limited distribution because of preliminary data, security classification, or other reasons.

CONTRACTOR REPORTS: Technical information generated in connection with a NASA contract or grant and released under NASA auspices.

TECHNICAL TRANSLATIONS: Information published in a foreign language considered to merit NASA distribution in English.

TECHNICAL REPRINTS: Information derived from NASA activities and initially published in the form of journal articles.

SPECIAL PUBLICATIONS: Information derived from or of value to NASA activities but not necessarily reporting the results of individual NASA-programmed scientific efforts. Publications include conference proceedings, monographs, data compilations, handbooks, sourcebooks, and special bibliographies.

Details on the availability of these publications may be obtained from:

SCIENTIFIC AND TECHNICAL INFORMATION DIVISION

NATIONAL AERONAUTICS AND SPACE ADMINISTRATION

Washington, D.C. 20546